

Efficient Gaussian Process Classification-based Physical-Layer Authentication with Configurable Fingerprints for 6G-Enabled IoT

Rui Meng, Fangzhou Zhu, Xiaodong Xu, *Senior Member, IEEE*,
 Bizhu Wang, Bingxuan Xu, and Ping Zhang, *Fellow, IEEE*

Abstract—The future 6G-enabled IoT will facilitate seamless global connectivity among ubiquitous wireless devices, but this advancement also introduces heightened security risks such as spoofing attacks. Physical-Layer Authentication (PLA) has emerged as a promising, inherently secure, and energy-efficient technique for authenticating IoT terminals. However, applying state-of-the-art PLA schemes directly to 6G-enabled IoT faces two primary challenges: inaccurate channel fingerprints and inefficient utilization of prior fingerprint information. To tackle these challenges, we leverage Intelligent Reflecting Surfaces (IRSs) to enhance fingerprint accuracy. Additionally, we integrate active learning and Gaussian Processes (GPs) to propose an Efficient Gaussian Process Classification (EGPC)-based PLA scheme, aiming for reliable and lightweight authentication. Following Bayes' theorem, we model configurable fingerprints using GPs and employ the Expectation Propagation (EP) method to identify unknown fingerprints. Given the difficulty of obtaining sufficient labeled fingerprint samples to train PLA models, we propose three fingerprint selection algorithms. These algorithms select unlabeled fingerprints whose identities are then queried to upper-layer authentication mechanisms. Among these methods, the optimal algorithm reduces the required number of training fingerprints through importance sampling and eliminates the need for PLA model retraining via joint distribution calculation. The simulations conducted on synthetic datasets demonstrate that the IRS-assisted PLA framework reduces the authentication error rate by 98.69% compared to the non-IRS-based approach. Furthermore, our proposed fingerprint selection algorithms achieve the reduction in the authentication error rate of up to 86.93% compared to baseline active learning algorithms.

Index Terms—Physical-Layer Authentication (PLA), 6G, IoT, identity security, Intelligent Reflecting Surface (IRS).

I. INTRODUCTION

AS AN extended and expanded system network based on the Internet, Internet of Things (IoT) can realize intelligent perception, recognition, and management of things and machine leveraging various devices and technologies, such as sensor equipment, global positioning system, infrared sensor, and laser scanner [1]. To advance IoT's ultimate goal

Corresponding author: Xiaodong Xu.

Rui Meng, Fangzhou Zhu, Bizhu Wang, and Bingxuan Xu are with the State Key Laboratory of Networking and Switching Technology, Beijing University of Posts and Telecommunications, Beijing 100876, China (e-mail: buptmen-grui@bupt.edu.cn; zfz9941@bupt.edu.cn; wangbizhu_7@bupt.edu.cn; xubingxuan@bupt.edu.cn).

Xiaodong Xu and Ping Zhang are with the State Key Laboratory of Networking and Switching Technology, Beijing University of Posts and Telecommunications, Beijing 100876, China, and also with the Department of Broadband Communication, Peng Cheng Laboratory, Shenzhen 518066, Guangdong, China (e-mail: xuxiaodong@bupt.edu.cn; pzhong@bupt.edu.cn).

of enabling real-time interaction among things, machines, and people, the 6th generation mobile network (6G) promises enhanced services surpassing those of 5G. These improvements include seamless coverage, higher data rates, and intrinsic security enhancements. Achieving this will involve implementing multi-band ultrafast-speed transmission, a highly adaptable integrated network, multi-node multi-domain joint transmission, and intelligent transmission mechanisms. [2].

Nevertheless, the worldwide seamless integration of IoT enabled by 6G necessitates an increased involvement of radio equipment in communication processes. This expansion of the application field, however, also introduces heightened security risks of a more pressing nature [3]. Besides, owing to the wireless transmission media's open broadcast nature, more aggressors may fabricate identification information to pretend to be legitimate users and further modify their privacy information [4]. Hence, the lightweight and efficient identity authentication plays a crucial role in achieving seamless and trustworthy communication [5]. Currently, the identity identification of terminals in 5G systems is mainly achieved by the core network, which adopts the authentication mechanisms based on cryptography, such as 5G Authentication and Key Agreement (5G AKA) [6]. Although the above cryptographic techniques at the upper layers have been incorporated into the 5G standard, they may fail to meet the expected performance levels in various emerging applications integrating 6G and IoT due to the constrained security level [7], low compatibility between heterogeneous systems [8], and unbearable computational overhead for IoT terminals with limited resources [9].

Consequently, to ensure high-reliable communications in 6G-enabled IoT, more efficient and reliable terminal access authentication approaches are required. Recently, Physical-Layer Authentication (PLA) has emerged as a complement of the above traditional security mechanisms, offering the following strengths.

- First of all, unlike the “patch” and “plugin” cryptography techniques at the upper-layers [10], PLA is designed based on physical-layer features that are exploited from the communication links, devices, and location-related attributes, such as Channel State Information (CSI) [11], [12], Received Signal Strength (RSS) [4], [9], peak power (PP) [13], and RF fingerprints [14]. These physical quantities are regarded as inherent fingerprints, possessing unique characteristics such as temporal variability, randomness, and spatial independence within radio channels

[10], [12]. That is to say, endogenous fingerprints at the physical-layer can provide particular identifying signatures and natural dynamic protection for legitimate IoT terminals, and extracting these channel characteristics and forging them presents an immensely formidable challenge for adversaries [15].

- Besides, PLA is a lightweight method circumventing many upper-layer signaling processes, leading to improved efficiency. During the channel estimation phase, the access point obtains all authorized users' CSI information, which further reduces computational overhead. Consequently, IoT devices with limited computing and storage resources can perform optimally [7].
- In addition, PLA exhibits high compatibility in heterogeneous coexistence environments. While incompatible devices may struggle to decode each other's upper-layer signaling, they should still be capable of decoding the bit-streams at the physical layer. PLA utilizes the physical-layer characteristics of devices for identification and verification, independent of software and protocols. It ensures a consistent experience through unified authentication standards, customizable to specific needs [16].

In earlier literature, PLA is formulated as statistical hypothesis testing, where estimated fingerprints are identified as legitimate when the differences between them and the reference vector do not exceed the detection threshold [17]. However, due to the challenges in accurately modeling the fingerprint distribution of IoT terminals caused by unknown and uncertain dynamic variation in 6G systems, obtaining the theoretically optimal threshold becomes difficult [18]. Machine Learning (ML)-based PLA approaches have recently garnered more interest, as intelligent algorithms possess powerful feature learning abilities that enhance authentication reliability and robustness [19]. Various ML techniques are employed to capture the differences between legal and illegal fingerprints, such as the Gaussian kernel method [18], support vector machine [20], weighted voting [21], neural networks [12], [22], and reinforcement learning [23]. Intelligent PLA technologies can be employed in one of six usage scenarios of 6G recommended by International Telecommunication Union (ITU): artificial intelligence and communication [24].

Nevertheless, there are two challenges of applying existing ML-based PLA schemes directly to 6G-empowered IoT:

- The first challenge is the inaccurate channel fingerprints within complex wireless environments. These fingerprints serve as crucial identifiers for IoT terminals, requiring high precision to exhibit distinct features essential for authentication. However, in low Signal-to-Noise Ratio (SNR) scenarios influenced by electromagnetic interference, lengthy transmission paths, and multipath effects, inaccurate fingerprint estimation significantly impairs identification performance [16]. While multi-attribute [4], [25], [26] and multi-observation [13], [21], [27], [28] approaches enhance the distinguishability of legitimate IoT terminals, the fundamental challenge of fingerprint estimation remains unresolved. In fact, these approaches may introduce new issues, such as increased deployment

costs and security considerations associated with multi-receiver setups.

- The second challenge involves the inefficient utilization of prior information of fingerprints. Supervised learning-based PLA schemes depend on expert databases of fingerprints to train models effectively. However, obtaining identity labels through upper-layer authentication mechanisms escalates computational costs as the number of training samples increases. Moreover, not all training samples contribute equally to feature learning, extraction, and analysis; some may be redundant or trivial. Although semi-supervised learning approaches like variational autoencoders [29], clustering [4], and one-class classifiers [20], [27] circumvent the need for attacker-specific prior information, they face limitations in detecting attacks due to the absence of labeled attacker fingerprints for guiding model training.

In response to these challenges, we utilize Intelligent Reflecting Surfaces (IRSs) to establish an alternative transmission path that offers improved channel quality, thereby enhancing the reliability of channel fingerprints. IRSs represent a pioneering technology in 6G, employing a planar array of cost-effective reflective elements to dynamically manipulate the phase, amplitude, or frequency of incoming signals, thus significantly boosting overall communication performance [30]. IRSs are primarily controlled by base stations (BSs) to extend coverage, especially in high-frequency bands such as millimeter waves. Importantly, these deployments also hold promise for authentication purposes. For example, Gao et al. [31] combine IRSs and key-based authentication approaches to improve the key generation rate. Furthermore, we leverage Gaussian processes (GPs) [32] to model configurable fingerprints introduced by IRSs for the following reasons: GPs possess the flexibility to model complex and nonlinear relationships and offer a probabilistic depiction of model uncertainty. Given that various optimization approaches [33] can dynamically adjust the parameters of IRSs for resource allocation and energy efficient maximization, the statistical characteristics of channels vary over time and space. GPs are adept at capturing these variations and handling uncertainties, thereby effectively fitting the fingerprint distribution. For instance, Wang et al. [20] utilize GP regression to predict mobile transmitters' CSI fingerprints. Moreover, to efficiently utilize prior fingerprint information for guiding the training of PLA models, we employ active learning [34] to facilitate interaction between PLA and upper-layer authentication mechanisms. The fingerprint selection algorithm chooses representative unlabeled fingerprints, which are then tagged with identity labels through upper-layer authentication mechanism, thereby guiding the training of the PLA model. This iterative process enables the achievement of robust PLA models with a minimal set of labeled training fingerprints. To provide a concise summary, the primary contributions are outlined as follows:

- We introduce an Efficient Gaussian Process Classification (EGPC)-based PLA scheme for 6G-enabled IoT to realize lightweight and reliable cross-layer identity recognition. IRSs are utilized to obtain configurable fingerprints with

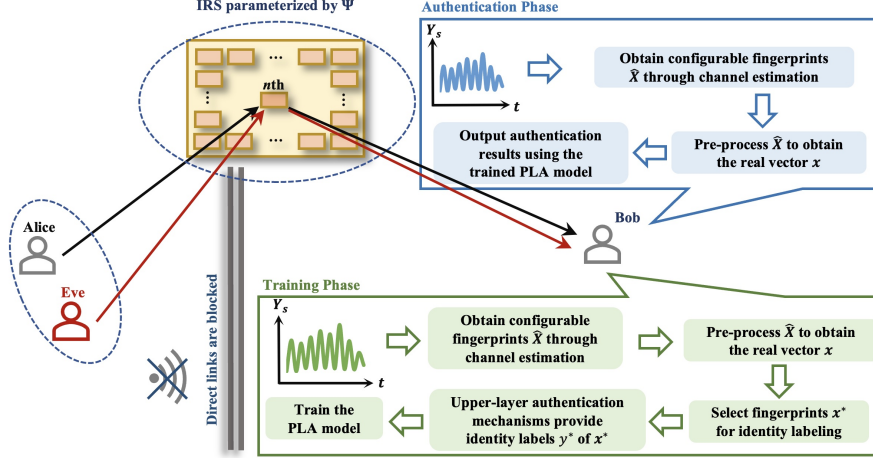


Fig. 1. The designed EGPC-based PLA scheme, where Alice and Eves respectively are legal and spoofing transmitters, and Bob is responsible for identity recognition.

enhanced accuracy. Active learning is employed to selectively label these fingerprints, thereby maximizing the utilization efficiency of existing fingerprint data.

- Configurable fingerprints are modeled using GPs in our proposed Gaussian Process Classification (GPC)-based PLA approach. Additionally, we leverage the Expectation Propagation (EP) method to approximate the posterior prediction of unknown fingerprint identities.
- We present three fingerprint selection algorithms, including Random Optimization (RO), Average Loss of Uncertainty (ALU), and Soft-ALU (SALU). These algorithms select the most uncertain fingerprint sample from an unlabeled pool for prioritized labeling. The design enhances interaction efficiency between PLA and upper-layer authentication mechanisms.
- Simulations conducted on synthetic dataset demonstrate the effectiveness of our proposed scheme. Moreover, our algorithms are shown to outperform three baseline active learning algorithms in terms of authentication error rate.

II. SYSTEM MODEL AND PROBLEM FORMULATION

A. Network Model

As shown in Fig. 1, a typical security model is considered, which is described as follows.

- Alice (legal IoT terminal):** This paper concentrates on the authentication of uplink channel signals. Alice transmits signals to Bob for identity authentication requests.
- Eve (spoofing attacker):** Eve attempts to impersonate Alice and transmit signals to Bob during different communication time slots. The position of Eve is assumed to be more than half a wavelength away from Alice for strong spatial decorrelation between their fingerprints.
- Bob (BS):** Bob is tasked with identifying the identities of received signals. The ML-based PLA model is trained and deployed at Bob. The training process can benefit from edge computing assistance.
- IRS:** The accuracy and reliability of fingerprints in low SNR environments are inherently limited, thus impacting the performance of PLA methods. In such scenarios, IRSs

can facilitate wireless connectivity between Alice and Bob. Through configurable adjustments of IRS settings, Bob can effectively manipulate the channel between Alice, thereby bolstering the spatial discernibility of fingerprints. The integration of IRSs within authentication protocols presents significant potential, particularly within controlled settings such as smart factories [35]. Incorporating IRSs within authentication procedures enhances security measures, ensuring robust identity verification and access control [36]. The absence of direct links between transmitters and Bob is assumed for simplicity.

TABLE I
THE LIST OF MAIN PARAMETERS

Notations	Meaning
\mathbb{E}	Expectation
\mathbb{V}	Variance
\propto	Proportional to
\sim	Distributed according to
\mathbf{x}^T	The transpose of vector \mathbf{x}
y	The identity label
$\sigma(z)$	The sigmoid function
\triangleq	An equality which acts as a definition
f_*	Gaussian process posterior prediction
\mathbf{X}_S	The transmitted signal vector
\mathbf{Y}_S	The received signal vector
$\mathbf{Q}^{(A,I,B)}$	The hierarchical channel matrix from Alice to Bob through IRS
Ψ	The matrix of IRS element responses
$\hat{\mathbf{X}}$	The estimated configurable fingerprints
$f(\mathbf{x})$ or \mathbf{f}	Gaussian process latent function values
$\bar{\pi}_*$	The probabilistic prediction of the identity
Z	The marginal likelihood
$\Phi(z)$	The CDF of a standard normal distribution
$t_i(f_i \hat{Z}_i, \hat{\mu}_i, \hat{\sigma}_i^2)$	The local likelihood approximation
$q(\mathbf{f} \mathbf{X}, \mathbf{y})$	The distribution posterior used to approximate $p(\mathbf{f} \mathbf{X}, \mathbf{y})$
K	The covariance (or Gram) matrix
\mathbf{k}_*	Short for $K(\mathbf{X}, \mathbf{x}_*)$
$q_{-i}(f_i)$	The cavity distribution

B. Channel Model

Let N_T and N_R denote the number of antennas of Alice and Bob, respectively. The received signal vector with N_R -size column \mathbf{Y}_S at Bob can be represented as

$$\mathbf{Y}_S = \mathbf{Q}^{(A,I,B)} \mathbf{X}_S + \mathbf{W}, \quad (1)$$

where \mathbf{X}_S is the signal vector with N_T -size column transmitted from Alice and $\mathbf{W} \sim \mathcal{CN}(0, \sigma^2)$ is the Gaussian noise vector with N_R -size column. Denoting the number of elements of IRS by N , $\mathbf{Q}^{(A,I,B)} = \mathbf{H}\Psi\mathbf{G}$ is the hierarchical channel matrix from Alice to Bob through IRS, where \mathbf{H} and \mathbf{G} represent the channel matrix with $N_R \times N$ from IRS to Bob and the channel matrix with $N \times N_T$ from Alice to IRS, respectively. $\Psi = \text{diag}(\psi_0, \dots, \psi_{N-1})$ is the matrix of IRS element responses. φ_n is represented as $\varphi_n = A_n(\theta_n) e^{j\theta_n}$, where $A_n(\theta_n)$ and $e^{j\theta_n}$ denote the controllable magnitude and phase response of the n th IRS element, respectively. The configurable fingerprints $\hat{\mathbf{X}}$ are obtained through

$$\hat{\mathbf{X}} = f_{ce}(\mathbf{Y}_S), \quad (2)$$

where f_{ce} denotes the channel estimation function. The channel estimation is not the focus of this paper and can be achieved by various methods, including classical channel estimation, compressed sensing, matrix factorization, and deep learning approaches [37].

C. Problem Formulation

We pre-process $\hat{\mathbf{X}}$ and then obtain the $2N_R N_T$ -dimensional real vector \mathbf{x} . Denote the configurable fingerprint space and the identity label set by \mathcal{X} and \mathcal{Y} , respectively. Our objective is to train an authentication system $\psi : \mathcal{X} \rightarrow \mathcal{Y}$ to predict the identities of unknown fingerprints $\psi(\mathbf{x}_*)$ ($\mathbf{x}_* \in \mathcal{X}$), which will be discussed in Sec. III.

Given that IRSs introduce a more intricate signal processing framework, and that the identity labeling of fingerprints requires involvement in the upper authentication protocol, it becomes crucial to devise an efficient fingerprint labeling strategy. This strategy is formulated as

$$f_{fl} = (\mathcal{U}, \mathcal{L}), \quad (3)$$

where \mathcal{U} and \mathcal{L} represent unlabeled and labeled fingerprints, respectively, and f_{fl} is the fingerprint labeling function. f_{fl} outputs the selected unlabeled fingerprints $x^* \in \mathcal{U}$ for identity labeling. Through iterative selection and labeling, the reliability of the PLA model is progressively enhanced. The fingerprint labeling strategy will be discussed in Sec. IV. The main parameters are illustrated in Tab. I.

III. POSTERIOR PREDICTION OF UNKNOWN CONFIGURABLE FINGERPRINTS

GP is a robust non-parametric method capable of dynamically adapting to complex and varying channel conditions, effectively capturing and modeling their intricacies. Moreover, GP can adeptly handle the uncertainty inherent in channel characteristics across time, space, and frequency domains through its Bayesian framework, making it ideal for fitting

configurable fingerprints' distributions. Hence, this section introduces a GPC-based PLA model to derive posterior predictions of fingerprints.

A. GPs for Configurable Fingerprints

As discussed in Sec. II-C, the identity recognition problem is formulated as a classification function ψ that assigns the configurable fingerprints \mathbf{x} to one of two classes, $y = 0$ and $y = 1$, corresponding to Alice and Eve, respectively. We use a GPC framework to connect the configurable fingerprints and the identity labels via a latent function f following a GP prior $f \sim GP(\mu(\cdot), k(\cdot, \cdot))$, where $\mu(\cdot)$ and $k(\cdot, \cdot)$ are the mean function and covariance kernel function, respectively.

By "squashing" the GP prior function $f(\mathbf{x})$, we can obtain a prior on $\pi(\mathbf{x})p(y = +1 | \mathbf{x}) = \sigma(f(\mathbf{x}))$ through the logistic function. To remove (integrate out) $f(\mathbf{x})$, the distribution of the latent variable of an unknown configurable fingerprint is computed as

$$p(f_* | X, \mathbf{y}, \mathbf{x}_*) = \int p(f_* | X, \mathbf{x}_*, \mathbf{f}) p(\mathbf{f} | X, \mathbf{y}) d\mathbf{f}, \quad (4)$$

where $p(\mathbf{f} | X, \mathbf{y}) = p(\mathbf{y} | \mathbf{f}) p(\mathbf{f} | X) / p(\mathbf{y} | X)$ denotes the posterior over the hidden variables. Then, we can use $p(f_* | X, \mathbf{y}, \mathbf{x}_*)$ to obtain the probabilistic prediction of the identity as

$$\bar{\pi}_* \triangleq p(y_* = +1 | X, \mathbf{y}, \mathbf{x}_*) = \int \sigma(f_*) p(f_* | X, \mathbf{y}, \mathbf{x}_*) df_*. \quad (5)$$

The integral in (4) and (5) are analytically intractable because of the non-Gaussian likelihood. EP method [32] is further employed to approximate the non-Gaussian joint posterior.

B. Expectation Propagation-based Posterior Prediction

According to Bayes' rule, the posterior $p(\mathbf{f} | X, \mathbf{y})$ is denoted as

$$p(\mathbf{f} | X, \mathbf{y}) = \frac{1}{Z} p(\mathbf{f} | X) \prod_{i=1}^n p(y_i | f_i), \quad (6)$$

where $p(\mathbf{f} | X)$ denotes the Gaussian prior, $\prod_{i=1}^n p(y_i | f_i)$ represents the likelihood, and n is the number of the training fingerprint samples. We can obtain marginal likelihood as

$$Z = p(\mathbf{y} | X) = \int p(\mathbf{f} | X) \prod_{i=1}^n p(y_i | f_i) d\mathbf{f}. \quad (7)$$

To make $p(\mathbf{f} | X, \mathbf{y})$ analytically intractable, we utilize the probit likelihood as

$$p(y_i | f_i) = \Phi(f_i y_i), \quad (8)$$

where $\Phi(z) = \int_{-\infty}^z \mathcal{N}(x | 0, 1) dx$ is the cumulative density function (CDF) of the standard Gaussian distribution. The likelihood $\Phi(f_i y_i)$ is approximated through the local likelihood approximation as

$$p(y_i | f_i) \simeq t_i \left(f_i \middle| \tilde{Z}_i, \tilde{\mu}_i, \tilde{\sigma}_i^2 \right) = \tilde{Z}_i \mathcal{N}(f_i | \tilde{\mu}_i, \tilde{\sigma}_i^2), \quad (9)$$

where \tilde{Z}_i , $\tilde{\mu}_i$, and $\tilde{\sigma}_i^2$ are site parameters, and the local likelihoods t_i satisfy

$$\prod_{i=1}^n t_i \left(f_i \mid \tilde{Z}_i, \tilde{\mu}_i, \tilde{\sigma}_i^2 \right) = \mathcal{N} \left(\tilde{\mu}, \tilde{\Sigma} \right) \prod_i \tilde{Z}_i, \quad (10)$$

where $\tilde{\mu}$ denotes the vector of $\tilde{\mu}_i$ and $\tilde{\Sigma}$ is diagonal with $\tilde{\Sigma}_{ii} = \tilde{\sigma}_i^2$.

We can approximate the posterior of $p(\mathbf{f}|X, \mathbf{y})$ as

$$q(\mathbf{f}|X, \mathbf{y}) \triangleq \frac{1}{Z_{EP}} p(\mathbf{f}|X) \prod_{i=1}^n t_i \left(f_i \mid \tilde{Z}_i, \tilde{\mu}_i, \tilde{\sigma}_i^2 \right) = \mathcal{N}(\boldsymbol{\mu}, \boldsymbol{\Sigma}), \quad (11)$$

where $\boldsymbol{\mu} = \Sigma \tilde{\Sigma}^{-1} \tilde{\mu}$ and $\boldsymbol{\Sigma} = (K^{-1} + \tilde{\Sigma}^{-1})^{-1}$. K is a $n \times n$ covariance matrix. $Z_{EP} = q(\mathbf{y}|X)$ denotes the approximation to Z from (6) and (7).

Remark 1. To choose the parameters of t_i , one feasible approach is to minimize the reversed Kullback-Leibler (KL) divergence $KL(q(\mathbf{f}|X, \mathbf{y}) \parallel p(\mathbf{f}|X, \mathbf{y}))$ with respect to $q(\mathbf{f}|X, \mathbf{y})$, which is also known as the variational inference. In this paper, the EP method is used to update the approximation of t_i sequentially, which are discussed as follows.

1) *Marginal Cavity Distribution:* By combining $p(\mathbf{f}|X)$ and $\prod_{i=1}^n t_i \left(f_i \mid \tilde{Z}_i, \tilde{\mu}_i, \tilde{\sigma}_i^2 \right)$, we can obtain the cavity distribution as

$$q_{-i}(f_i) \propto \int p(\mathbf{f}|X) \prod_{j \neq i} t_j \left(f_j \mid \tilde{Z}_j, \tilde{\mu}_j, \tilde{\sigma}_j^2 \right) df_j. \quad (12)$$

We combine $p(\mathbf{f}|X)$ and the $(n-1)$ approximate likelihoods in (12) through equivalently removing $t_i \left(f_i \mid \tilde{Z}_i, \tilde{\mu}_i, \tilde{\sigma}_i^2 \right)$ from the approximated posterior $\prod_{i=1}^n t_i \left(f_i \mid \tilde{Z}_i, \tilde{\mu}_i, \tilde{\sigma}_i^2 \right)$ in (11).

Proposition 1. We can obtain the marginal distribution for f_i from $q(\mathbf{f}|X, \mathbf{y})$ as

$$q(f_i|X, \mathbf{y}) = \mathcal{N}(f_i|\mu_i, \sigma_i^2), \quad (13)$$

where $\sigma_i^2 = \Sigma_{ii}$.

Proof: See Appendix A. ■

Proposition 2. Through dividing (13) by t_i , we can obtain the cavity distribution as

$$q_{-i}(f_i) = \mathcal{N}(f_i|\mu_{-i}, \sigma_{-i}^2), \quad (14)$$

where $\mu_{-i} = \sigma_{-i}^2(\sigma_i^{-2}\mu_i - \tilde{\sigma}_i^{-2}\tilde{\mu}_i)$ and $\sigma_{-i}^2 = (\sigma_i^{-2} - \tilde{\sigma}_i^{-2})^{-1}$. ■

Proof: See Appendix B. ■

2) *The Gaussian Approximation to the Non-Gaussian Marginal Distribution:* The product of $q_{-i}(f_i)$ and $p(y_i|f_i)$ can be approximated by a non-normalized Gaussian marginal distribution, which is defined as

$$\hat{q}(f_i) \triangleq \hat{Z}_i \mathcal{N}(\hat{\mu}_i, \hat{\sigma}_i^2) \simeq q_{-i}(f_i) p(y_i|f_i). \quad (15)$$

Proposition 3. Considering that $\hat{q}(f_i)$ is un-normalized, to match $q_{-i}(f_i) p(y_i|f_i)$, the desired posterior marginal moments should satisfy

$$\hat{Z}_i = \Phi(z_i), \quad (16)$$

$$\hat{\mu}_i = \mu_{-i} + \frac{y_i \sigma_{-i}^2 \mathcal{N}(z_i)}{\Phi(z_i) \sqrt{1 + \sigma_{-i}^2}}, \quad (17)$$

and

$$\hat{\sigma}_i^2 = \sigma_{-i}^2 - \frac{\sigma_{-i}^4 \mathcal{N}(z_i)}{(1 + \sigma_{-i}^2) \Phi(z_i)} \left(z_i + \frac{\mathcal{N}(z_i)}{\Phi(z_i)} \right), \quad (18)$$

where $z_i = \frac{y_i \mu_{-i}}{\sqrt{1 + \sigma_{-i}^2}}$. ■

Proof: See Appendix C. ■

3) *The Computation of t_i :*

Proposition 4. multiplying $\hat{q}(f_i) = \hat{Z}_i \mathcal{N}(\hat{\mu}_i, \hat{\sigma}_i^2)$ by $q_{-i}(f_i) = \mathcal{N}(f_i|\mu_{-i}, \sigma_{-i}^2)$, the site parameters of $p(y_i|f_i) \simeq \hat{Z}_i \mathcal{N}(f_i|\tilde{\mu}_i, \tilde{\sigma}_i^2)$ in (9) are obtained as

$$\tilde{\mu}_i = \tilde{\sigma}_i^2 (\tilde{\sigma}_i^{-2} \hat{\mu}_i - \sigma_{-i}^{-2} \mu_{-i}), \quad (19)$$

$$\tilde{\sigma}_i^2 = (\hat{\sigma}_i^{-2} - \sigma_{-i}^{-2})^{-1}, \quad (20)$$

and

$$\tilde{Z}_i = \hat{Z}_i \sqrt{2\pi} \sqrt{\sigma_{-i}^2 + \tilde{\sigma}_i^2} \exp \left(\frac{(\mu_{-i} - \tilde{\mu}_i)^2}{2(\sigma_{-i}^2 + \tilde{\sigma}_i^2)} \right). \quad (21)$$

Proof: See Appendix D. ■

Thus, through iteratively moment matching marginal posteriors, we can approximate $p(\mathbf{f}|X, \mathbf{y})$ with the Gaussian approximation $q(\mathbf{f}|X, \mathbf{y})$.

Proposition 5. There exists a closed-form expression for $p(y_*|X, \mathbf{y}, \mathbf{x}_*)$ as

$$p(y_*|X, \mathbf{y}, \mathbf{x}_*) = \Phi \left(\frac{\mathbf{k}_*^T (K + \tilde{\Sigma})^{-1} \tilde{\mu}}{\sqrt{1 + k(\mathbf{x}_*, \mathbf{x}_*) - \mathbf{k}_*^T (K + \tilde{\Sigma})^{-1} \mathbf{k}_*}} \right), \quad (22)$$

where $\mathbf{k}_* = K(X, \mathbf{x}_*)$, \mathbf{k}_*^T denotes the transpose of \mathbf{k}_* , and $k(\mathbf{x}_*, \mathbf{x}_*)$ is covariance functions evaluated at \mathbf{x}_* and \mathbf{x}_* .

Proof: See Appendix E. ■

Given $p(y_*|X, \mathbf{y}, \mathbf{x}_*)$, the identity of unknown fingerprints \mathbf{x}_* is obtained according to $\arg \max_{y_*} p(y_*|X, \mathbf{y}, \mathbf{x}_*)$ [38].

IV. PROPOSED EGPC-BASED PLA SCHEME

In this section, building upon the proposed GPC-based PLA scheme in Sec. III, we present an active learning-based lightweight and efficient PLA approach. Additionally, we introduce three fingerprint selection algorithms designed to facilitate interaction between the PLA and upper-layer authentication mechanisms.

A. Active Learning-based Efficient Fingerprint Labeling

The state-of-the-art ML-based PLA schemes can be divided into two main categories: supervised learning-based and semi-supervised learning-based schemes. In supervised learning-based schemes, all fingerprint samples are labeled. However, acquiring sufficient labeled fingerprints in real-world wireless systems is often impractical due to attackers'

concealment. This challenge is exacerbated in IRS systems with dynamic programmable characteristics, where obtaining prior information about attackers becomes even more difficult. Conversely, semi-supervised learning schemes involve labeling only a subset of fingerprint samples. Yet, the scarcity of prior information poses difficulties in building a dependable and resilient authentication system. Specifically, similarities and redundancies in feature patterns among labeled fingerprints not only escalate computational labeling costs but also curtail the PLA model's generalization capability. The integration of IRSs further alters the fingerprint distribution, necessitating representative samples to effectively train an accurate authentication model.

To efficiently train a robust PLA model using a limited number of labeled configurable fingerprint samples, the selection of labeled configurable fingerprints is crucial. We employ active learning as a strategy to achieve this aim. As depicted in Fig. 2, active learning¹ usually assumes the availability of a small set of labeled data \mathcal{L} and a large pool of unlabeled data \mathcal{U} . The learner can pose “queries”, usually in the form of unlabeled samples to be labeled by an “oracle”, such as a human annotator. Queries are selected in a greedy manner based on a utility measure that evaluates all unlabeled samples in the pool. Active learning approaches have been extensively studied across various problems, such as image classification, video classification, information extraction, and text classification, to name only a few.

Remark 2. In practice, PLA does not replace upper-layer security mechanisms but rather complements them, thereby enhancing overall security [7], [15]. As detailed in **Algorithm 1**, inspired by active learning, the proposed EGPC-based PLA scheme involves continuous interaction with the upper-layer authentication protocol to iteratively update labeled fingerprints. Specifically, the fingerprint selection algorithm selects unlabeled fingerprint samples \mathbf{x}_* , whose identity labels are provided by upper-layer authentication mechanisms. The authentication model adjusts its parameters dynamically upon receiving new labeled fingerprint samples, continuing the learning process until achieving desired authentication performance. Hence, the lightweight cross-layer identification scheme enhances identity recognition efficiency and improves security. Obviously, the selection of \mathbf{x}_* influences the PLA model's training efficiency. In Sec. IV-B and IV-C, we will introduce three fingerprint selection algorithms to choose the most uncertain fingerprint sample \mathbf{x}_* from a set of unlabeled fingerprint samples \mathcal{U} .

B. Proposed RO-based Fingerprint Selection Algorithm

In each iteration, the optimal \mathbf{x}_* is selected through optimizing an acquisition function that is usually related to $\pi(\mathbf{f}|X, \mathbf{y})$. The Optimal Bayesian Classifier (OBC) [38] is

¹The paper primarily focuses on pool-based active learning, which is one of the three major scenarios in active learning. The other scenarios include membership query synthesis and stream-based selective sampling.

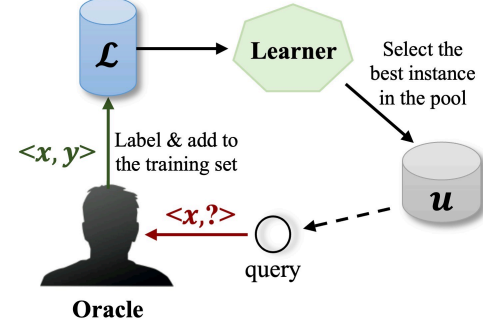


Fig. 2. Illustration of the pool-based active learning.

Algorithm 1 Steps of the Proposed EGPC-based PLA Scheme

Input: \mathcal{U} : unlabeled fingerprint samples $\{\mathbf{x}^{(u)}\}_{u=1}^U$; \mathcal{L} : initially labeled fingerprint samples $\{<\mathbf{x}, y>^{(l)}\}_{l=1}^L$

Process:

- 1: **for** $t = 1, 2, \dots$ **do**
- 2: Train the authentication system θ through the GPC-based scheme in Sec. III;
- 3: Select $\mathbf{x}^* \in \mathcal{U}$ based on **Algorithm 2 or 3**;
- 4: Query the upper-layer security mechanisms to obtain the identity of fingerprints \mathbf{x}^* , that is, label y^* ;
- 5: Add $<\mathbf{x}^*, y^*>$ to \mathcal{L} ;
- 6: Remove \mathbf{x}^* from \mathcal{U}
- 7: **end for**

Output: The trained authentication system

represented by $\psi_{\pi(\mathbf{f})}(\cdot)$. The expected authentication error of the OBC can be denoted as

$$\begin{aligned} & \mathbb{E}_{\mathbf{x}_s} \{1 - p(y_s = \psi_{\pi(\mathbf{f})}(\mathbf{x}_s) | \mathbf{x}_s)\} \\ &= \mathbb{E}_{\mathbf{x}_s} \left\{ 1 - \max_{y_s} p(y_s | \mathbf{x}_s) \right\}. \end{aligned} \quad (23)$$

We first randomly sample fingerprint set $\mathcal{X}_* \subset \mathcal{X}$ with the size of M_1 , calculate the acquisition function, and then choose the fingerprint sample as the optimal \mathbf{x}_* . Define $U^A(\mathbf{x}_*) = \mathbb{E}_{\mathbf{x}_s} \{g^A(\mathbf{x}_s; \mathbf{x}_*)\}$ and $U^S(\mathbf{x}_*) = \mathbb{E}_{\mathbf{x}_s} \{g^S(\mathbf{x}_s; \mathbf{x}_*)\}$. We denote either $g^A(\mathbf{x}_s; \mathbf{x}_*)$ or $g^S(\mathbf{x}_s; \mathbf{x}_*)$ by $g(\mathbf{x}_s; \mathbf{x}_*)$ that can be calculated if we know $p(y_s | \mathbf{x}_s)$ and $p(y_s | \mathbf{x}_s, \mathbf{x}_*, y_*)$. Through iteratively retraining the GPC-based authentication model by the EP method, the acquisition function is optimized. The steps of the RO-based fingerprint selection algorithm is shown in **Algorithm 2**.

C. Proposed ALU-based and SALU-based Fingerprint Selection Algorithms

Remark 3. There are two issues for **Algorithm 2** in actual communications as follows. 1) The number of fingerprints M_2 is large to guarantee the highly-reliable approximation of the integral in (24). 2) The calculation of $p(y_s | \mathbf{x}_s, \mathbf{x}_*, y_*)$ relies on retraining the GPC-based PLA model, which has high computational complexity $O(M_1 n^3)$. To address these two problems, we propose ALU-based and SALU-based fingerprint selection algorithms, which 1) reduce the required number of fingerprint samples through importance sampling,

$$U^S(\mathbf{x}_*) = \mathbb{E}_{\mathbf{x}_s} \left\{ \mathbb{E}_{y_*|\mathbf{x}_*} \left[\frac{1}{k} \log \text{SumExp}(k \cdot p(y_s | \mathbf{x}_s, \mathbf{x}_*, y_*)) \right] - \frac{1}{k} \log \text{SumExp}(k \cdot p(y_s | \mathbf{x}_s)) \right\} \quad (28)$$

Algorithm 2 Steps of the Proposed RO-based Fingerprint Selection Algorithm

Input: $p(\mathbf{x})$; $q(\mathbf{f}|X, \mathbf{y})$

Process:

- 1: Sample M_1 fingerprint samples of $\mathbf{x}_* \sim p(\mathbf{x})$, and sample M_2 fingerprint samples of $\mathbf{x}_s \sim p(\mathbf{x})$
- 2: **for** each \mathbf{x}_* **do**
- 3: Calculate $p(y_*|\mathbf{x}_*)$ by (22)
- 4: **for** y_* in $\{0, 1\}$ **do**
- 5: Approximate $q(\mathbf{f}|\mathbf{x}_*, y_*)$ by (19), (20), and (21)
- 6: **for** each \mathbf{x}_s **do**
- 7: Calculate $p(y_s|\mathbf{x}_s)$ and $p(y_s|\mathbf{x}_s, \mathbf{x}_*, y_*)$
- 8: Calculate $g(\mathbf{x}_s; \mathbf{x}_*)$
- 9: **end for**
- 10: **end for**
- 11: $U(\mathbf{x}_*) = \frac{1}{M_2} \sum_{\mathbf{x}_s} g(\mathbf{x}_s; \mathbf{x}_*)$
- 12: **end for**
- Output:** $\tilde{\mathbf{x}} = \arg \max_{\mathbf{x}_*} U(\mathbf{x}_*)$

and 2) avoid the retraining of the GPC-based PLA model through the joint distribution calculation.

Definition 1. Motivated by Mean objective Cost of Uncertainty (MOCU) [39], we define ALU as the expected loss difference between the OBC and the optimal classifier as

$$\begin{aligned} \mathcal{A}(\pi(\mathbf{f})) &\triangleq \mathbb{E}_{\mathbf{x}_s} \left\{ 1 - \max_{y_s} p(y_s | \mathbf{x}_s) \right\} \\ &\quad - \mathbb{E}_{\pi(\mathbf{f})} \left\{ \mathbb{E}_{\mathbf{x}_s} \left[1 - \max_{y_s} p(y_s | \mathbf{x}_s, \mathbf{f}) \right] \right\}. \end{aligned} \quad (24)$$

The ALU reduction is taken as the acquisition function as

$$U^A(\mathbf{x}_*; \pi(\mathbf{f})) = \mathcal{A}(\pi(\mathbf{f})) - \mathbb{E}_{y_*|\mathbf{x}_*} [\mathcal{A}(\pi(\mathbf{f}|\mathbf{x}_*, y_*))]. \quad (25)$$

According to [40], we can obtain

$$\begin{aligned} U(\mathbf{x}_*) &= \mathbb{E}_{\mathbf{x}_s} \left\{ 1 - \max_{y_s} p(y_s | \mathbf{x}_s) \right\} \\ &\quad - \mathbb{E}_{y_*|\mathbf{x}_*} \left\{ \mathbb{E}_{\mathbf{x}_s} \left[1 - \max_{y_s} p(y_s | \mathbf{x}_s, \mathbf{x}_*, y_*) \right] \right\} \\ &= \mathbb{E}_{\mathbf{x}_s} \left\{ \mathbb{E}_{y_*|\mathbf{x}_*} \left[\max_{y_s} p(y_s | \mathbf{x}_s, \mathbf{x}_*, y) \right] - \max_{y_s} p(y_s | \mathbf{x}_s) \right\}, \end{aligned} \quad (26)$$

which is also the expected error reduction of OBC [41].

Definition 2. Inspired by Soft-MOCU [42], we further define SALU in (27), a smooth concave approximation of ALU.

$$\begin{aligned} \mathcal{A}^S(\pi(\mathbf{f})) &\triangleq \mathbb{E}_{\mathbf{x}_s} \left\{ 1 - \frac{1}{k} \text{LogSumExp}(k \cdot p(y_s | \mathbf{x}_s)) \right\} \\ &\quad - \mathbb{E}_{\pi(\mathbf{f})} \left\{ \mathbb{E}_{\mathbf{x}_s} \left[1 - \max_{y_s} p(y_s | \mathbf{x}_s, \mathbf{f}) \right] \right\}. \end{aligned} \quad (27)$$

The corresponding acquisition function is denoted as (28), which has no maximization operators. After defining acquisition functions as (26) or (28), importance sampling and joint distribution calculation are employed as follows.

Algorithm 3 Steps of the Proposed ALU-based and SALU-based Fingerprint Selection Algorithms

Input: $p(\mathbf{x})$; $q(\mathbf{f}|X, \mathbf{y})$

Process:

- 1: Sample M_1 fingerprint samples of $\mathbf{x}_* \sim p(\mathbf{x})$
- 2: **for** each \mathbf{x}_* **do**
- 3: Calculate $p(y_*|\mathbf{x}_*)$ by (22)
- 4: Sample M_2 fingerprint samples of $\mathbf{x}_s \sim \tilde{p}(\mathbf{x}_s; \mathbf{x}_*)$
- 5: **for** y_* in $\{0, 1\}$ **do**
- 6: **for** each \mathbf{x}_s **do**
- 7: Calculate $p(y_s|\mathbf{x}_s, \mathbf{x}_*, y_*)$ by (31)
- 8: Calculate $p(y_s|\mathbf{x}_s)$ by (22)
- 9: Calculate $p(y_s|\mathbf{x}_s, \mathbf{x}_*, y_*) = \frac{p(y_s, y_*|\mathbf{x}_s, \mathbf{x}_*)}{p(y_s|\mathbf{x}_s)}$
- 10: Calculate $g(\mathbf{x}_s; \mathbf{x}_*)$
- 11: **end for**
- 12: **end for**
- 13: $U(\mathbf{x}_*) = \frac{1}{M_2} \sum_{\mathbf{x}_s} \frac{p(\mathbf{x}_s)g(\mathbf{x}_s; \mathbf{x}_*)}{\tilde{p}(\mathbf{x}_s; \mathbf{x}_*)}$
- 14: **end for**
- Output:** $\tilde{\mathbf{x}} = \arg \max_{\mathbf{x}_*} U(\mathbf{x}_*)$

1) *Importance Sampling:* $U(\mathbf{x}_*) = \mathbb{E}_{\mathbf{x}_s \sim p(\mathbf{x}_s)} [g(\mathbf{x}_s; \mathbf{x}_*)]$ can be reformulated over the distribution $\tilde{p}(\mathbf{x}_s; \mathbf{x}_*)$ as

$$U(\mathbf{x}_*) = \mathbb{E}_{\mathbf{x}_s \sim \tilde{p}(\mathbf{x}_s; \mathbf{x}_*)} \left[\frac{p(\mathbf{x}_s)g(\mathbf{x}_s; \mathbf{x}_*)}{\tilde{p}(\mathbf{x}_s; \mathbf{x}_*)} \right] \quad (29)$$

Assuming $\tilde{p}(\mathbf{x}_s; \mathbf{x}_*) \propto k(\mathbf{x}_s; \mathbf{x}_*)p(\mathbf{x}_s)$, we can obtain $p(y_s|\mathbf{x}_s, \mathbf{x}_*, y_*) \approx 0$ and $g(\mathbf{x}_s; \mathbf{x}_*) \approx 0$.

Considering that $k(\mathbf{x}_s; \mathbf{x}_*) \approx 0$, that is, $(\mathbf{x}_s; y_s)$ and $(\mathbf{x}_*; y_*)$ are independent, we can obtain $p(y_s|\mathbf{x}_s, \mathbf{x}_*, y_*) \approx 0$ and $g(\mathbf{x}_s; \mathbf{x}_*) \approx 0$.

2) *Joint Distribution Calculation:* To address the second issue in **Remark 3**, $p(y_s|\mathbf{x}_s, \mathbf{x}_*, y_*)$ is obtained as

$$p(y_s|\mathbf{x}_s, \mathbf{x}_*, y_*) = \frac{p(y_s, y_*|\mathbf{x}_s, \mathbf{x}_*)}{p(y_*|\mathbf{x}_*)}. \quad (30)$$

The calculation requires $p(y_s, y_*|\mathbf{x}_s, \mathbf{x}_*)$.

Proposition 6. The joint distribution $p(y_s, y_*|\mathbf{x}_s, \mathbf{x}_*)$ is expressed as

$$\begin{aligned} p(y_s = 1, y_* = 1 | \mathbf{x}_s, \mathbf{x}_*) &= \int \Phi \left(\frac{\tilde{\mu}_*(f_s)}{\sqrt{\tilde{\sigma}_{**} + 1}} \right) \Phi(f_s) \phi(f_s | \mu_s, \sigma_{ss}) df_s, \end{aligned} \quad (31)$$

where $f_s = f(\mathbf{x}_s)$, $f_* = f(\mathbf{x}_*)$, μ_{s*} and Σ_{s*} represent the marginal mean and covariance matrices of f_s and f_* , respectively. Denoting $\mu_{s*} = (\mu_s \ \mu_*)^\top$ and $\Sigma_{s*} = (\sigma_{ss} \ \sigma_{s*} \ \sigma_{s*} \ \sigma_{**})$, $\phi(f_s, f_* | \mu_{s*}, \Sigma_{s*}) = (f_s | \mu_s, \sigma_{ss}) (f_* | \tilde{\mu}_*(f_s), \tilde{\sigma}_{**})$, where $\tilde{\mu}_*(f_s) = \mu_* + \frac{(f_s - \mu_s)\sigma_{s*}}{\sigma_{ss}}$ and $\tilde{\sigma}_{**} = \sigma_{**} - \frac{\sigma_{s*}^2}{\sigma_{ss}}$.

Proof: See Appendix F. ■

The processes of the proposed (S)ALU-based fingerprint selection algorithms are shown in **Algorithm 3** in detail.

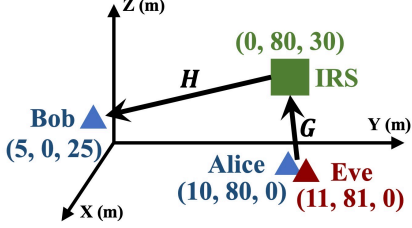


Fig. 3. The positions of Alice, Eve, Bob, and IRS.

V. PERFORMANCE EVALUATION AND SIMULATION RESULTS

A. Performance Metric

The authentication performance is measured by the authentication error rate R_e , which is represented as

$$R_e = \frac{1}{N_a} \sum_{n=1}^{N_a} \mathbb{I}(\mathbf{L}_n \neq \mathbf{Y}_n), \quad (32)$$

where N_a is the number of testing fingerprints, and \mathbf{L}_n and \mathbf{Y}_n respectively represent the true and estimated identities of the n th fingerprint. $\mathbb{I}(\cdot)$ takes 1 or 0 if \cdot is true or not, respectively.

Lemma 1. R_e is a fine-grained metric that incorporates both miss detection rate P_{md} and false alarm rate P_{fa} . R_e can be further denoted as

$$R_e = \frac{1}{1 + \frac{1}{\frac{1}{P_{md}} + \frac{1}{P_{fa}}}}, \quad (33)$$

where TL and TA are illustrated in Tab. II [4], [29].

Proof: See Appendix G. \blacksquare

TABLE II
CONFUSION MATRIX OF ALICE AND EVE

Actual \ Predicted	Alice	Eve
Alice	True Legitimate (TL)	False Attack (FA)
Eve	False Legitimate (FL)	True Attack (TA)

B. Simulation Parameters

Configurable fingerprint samples are generated through MATLAB platform. The positions of Alice, Eve, Bob, and IRS are illustrated in Fig. 3. Alice, Eve, and Bob are equipped with Uniform linear arrays, and the number of arrays of Alice/Eve and Bob are $N_T = 2$ and $N_R = 4$, respectively. IRS is a uniform rectangular array composed of $N = N_y N_z = 8 * 32$ reflective elements, and the distance between each reflective element is half wavelength. \mathbf{H} and \mathbf{G} are modeled as Rician Channels as

$$\mathbf{H} = \sqrt{\frac{PL_H^{LoS} \kappa_H}{1 + \kappa_H}} \bar{\mathbf{H}} + \sqrt{\frac{PL_H^{NLoS}}{1 + \kappa_H}} \tilde{\mathbf{H}} \quad (34)$$

$$\mathbf{G} = \sqrt{\frac{PL_G^{LoS} \kappa_G}{1 + \kappa_G}} \bar{\mathbf{G}} + \sqrt{\frac{PL_G^{NLoS}}{1 + \kappa_G}} \tilde{\mathbf{G}} \quad (35)$$

TABLE III
SIMULATION AND HYPER PARAMETERS

Parameters	Values
Bandwidth	1 MHz
Carrier Frequency f_c	3.5 GHz
Rice factors κ_h and κ_g	3 and 4
Number of IRS elements	8*32
Number of antennas of Bob N_R	4
Number of antennas of each transmitter N_T	2
Number of each transmitter's training fingerprints	800
Number of each transmitter's testing fingerprints	200
Learning rate	0.001
Iteration number	30
The variance of the RBF kernel	1
The length scale of the RBF kernel	0.4

where $\bar{\mathbf{H}}$ and $\bar{\mathbf{G}}$ are Line of Sight (LoS) paths, and $\tilde{\mathbf{H}}$ and $\tilde{\mathbf{G}}$ are Non-LoS (NLoS) paths. According to the 3GPP TR 38.901 [43], PL denotes the corresponding path loss as

$$PL_{LoS} = 32.4 + 21 \log_{10}(d) + 20 \log_{10}(f_c) \quad (36)$$

and

$$PL_{NLoS} = 32.4 + 31.9 \log_{10}(d) + 20 \log_{10}(f_c), \quad (37)$$

where d is the path's distance (in m), $f_c = 3.5$ GHz is the carrier frequency, and $\kappa_H = 3$ and $\kappa_G = 4$ are Rician factors. The bandwidth is 1 MHz. The LoS paths are modeled according to [44]. The NLoS paths are modeled as Rayleigh fading models, that is, each element of the channel matrix obeys the independent identically distributed variable $\mathcal{CN}(0, \mathbf{I})$. Artificial noises $\mathbf{W} \sim \mathcal{CN}(0, \sigma_w^2 \mathbf{I})$ are employed to model noisy wireless environments, where $\sigma_w^2 = 10^{-20}$.

The performance of PLA models is verified through the PyCharm platform. The synthetic fingerprint datasets are split into training and testing datasets. Initially two fingerprint samples are chosen from Alice and Eve for labeling and further used to estimate the GPC hyper-parameters. The learning procedures are repeated for 100 runs. The simulation and hyper parameters are shown in Tab. III in detail. The computer configurations are Intel Core i5-13600KF, 3.50 GHz basic frequency, and 32 GB of RAM.

C. Baseline Algorithms

The baseline fingerprint selection algorithms for performance comparison are as follows.

- Random Selection (RS): RS algorithm selects fingerprint samples randomly for labeling, with each sample having an equal sampling probability of being selected.
- Maximum Entropy Sampling (MES) [45]: MES algorithm chooses fingerprint samples based on Shannon entropy to maximize information gain.
- Bayesian Active Learning by Disagreement (BALD) [46]: BALD algorithm selects fingerprint samples that maximize the disagreement among posterior parameters regarding their outcome.

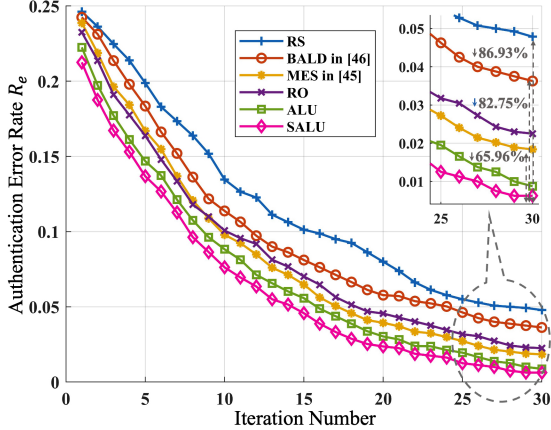


Fig. 4. Authentication error rate R_e versus different iteration numbers under IRS-assisted wireless environments.

D. Simulation Results

Comparisons with baseline algorithms. Fig. 4 compares the proposed fingerprint selection algorithms with three baseline active learning algorithms. As the iteration number increases, the proposed GPC-based PLA model observes more labeled fingerprint samples, gains a deeper understanding of configurable fingerprint distributions, and achieves more accurate predictions, thereby reducing authentication error rates. The analysis of the fingerprint selection algorithms is as follows. The RS algorithm selects fingerprints randomly, potentially choosing samples with similar characteristics repeatedly, limiting the PLA model's ability to learn the fingerprint distribution effectively. The BALD algorithm excels in learning the characteristics of low-dimensional data rather than high-dimensional fingerprints. The MES algorithm tends to prioritize querying points near decision boundaries, but multi-dimensional cascaded fingerprints have multiple boundaries. The proposed ALU algorithm uses expected error reduction as the acquisition function, outperforming the proposed RO algorithm in authentication performance. Compared to the ALU algorithm, the suggested SALU algorithm achieves a lower error rate due to its smoother concave approximation. Additionally, compared with the three baseline algorithms, the SALU algorithm reduces authentication error rates by 65.96% to 86.93%. Fig. 4 demonstrates the superior sampling efficiency of the proposed fingerprint selection algorithms over baseline active learning methods.

Effectiveness of IRSs. Fig. 5 presents the authentication performance in non-IRS and IRS-assisted wireless environments. In non-IRS environments with low SNRs, the channels between Alice/Eve and Bob are modeled as Rayleigh channels, characterized by severe fading. Across all iterations, the authentication error rate of the proposed fingerprint selection algorithms remains consistently around 0.5 in non-IRS scenarios. Due to the severe fading of the Rayleigh channel, there is significant overlap in the channel fingerprint space of Alice and Eve. Despite the gradual increase in labeled fingerprint samples, effectively learning the inherent characteristics of fingerprints remains challenging for the PLA model. In contrast, the channel quality improves with the transmission paths created by IRSs. With increasing iterations, an adequate

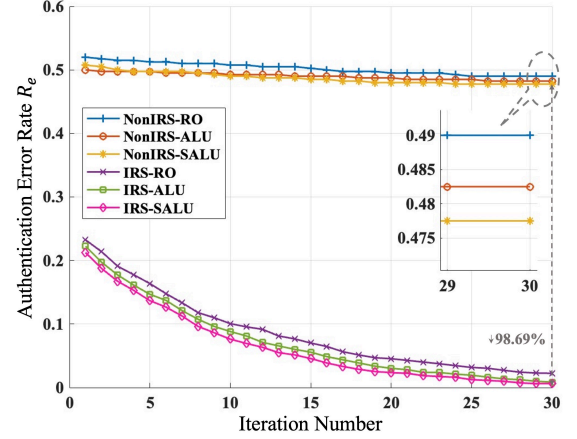


Fig. 5. Authentication error rate R_e versus different iteration numbers under non-IRS and IRS-assisted wireless environments.

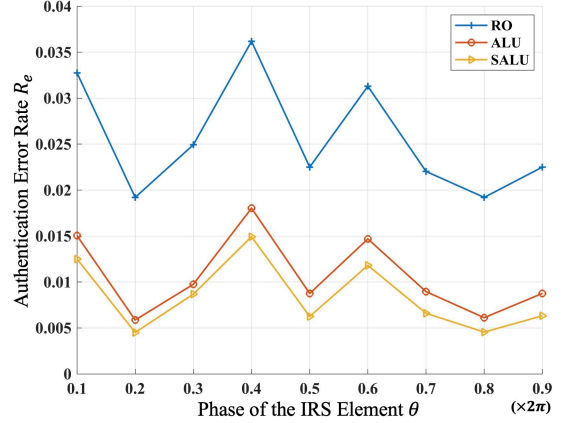


Fig. 6. Authentication error rate R_e versus different phase parameters of the IRS element θ .

number of labeled fingerprint samples significantly enhance authentication performance. Therefore, leveraging IRS assistance, the PLA model achieves superior authentication performance. For instance, compared to scenarios without IRS, the authentication error rate of the SALU algorithm with IRS assistance decreases by 98.69%. Fig. 5 shows the effectiveness of IRSs in enhancing authentication performance compared with the conventional non-IRS-based PLA framework under low SNR environments.

Performance versus IRS phase parameters. Fig. 6 provides the authentication performance versus different phase parameters of the IRS element $\theta = \theta_1 = \theta_2 = \dots = \theta_n$, where θ_n is the phase parameter of the n th IRS element. As the phase increases, the authentication error rate exhibits varying amplitudes. However, drawing definitive conclusions regarding IRS phase parameters and authentication error rates from Fig. 6 proves challenging. The optimization of IRS parameters is another important research area. Fig. 6 confirms that the selection of IRS phase parameters significantly impacts authentication performance.

Performance versus IRS columns numbers. Fig. 7 compares the authentication performance versus different numbers of columns of IRSs, denoted as N_z . As N_z increases, the total number of IRS element, $N = N_y N_z$, also increases. Consequently, the dimensions of \mathbf{H} , $\mathbf{\Psi}$, and \mathbf{G} in the cas-

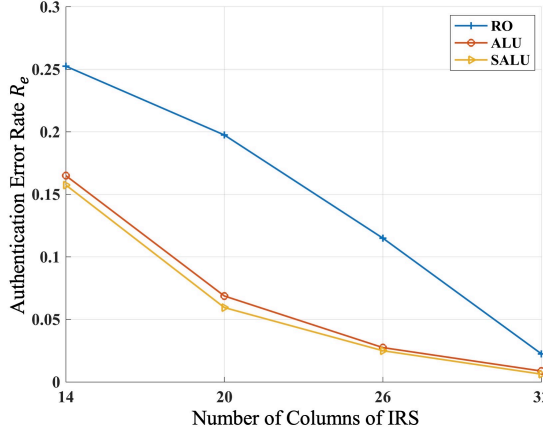


Fig. 7. Authentication error rate R_e versus different IRS column numbers.

cade channel matrix $Q^{(A,I,B)} = \mathbf{H}\Psi\mathbf{G}$ expand. When the dimensions of \mathbf{H} , Ψ , and \mathbf{G} are small, the limited variability in fingerprint distribution may not be enough to distinguish transmitters consistently. Conversely, with larger dimensions of \mathbf{H} , Ψ , and \mathbf{G} , it is more challenging for attackers to predict or imitate each component of fingerprints. Fig. 7 verifies a greater number of IRS columns contributes to enhanced authentication performance.

Performance under different SNRs. Although Fig. 5 demonstrates the efficacy of IRSs in improving authentication performance, channel fingerprint estimation is susceptible to biases from noises in channels between Alice/Eve and IRSs, or between IRSs and Bob. To analyze authentication performance under varying channel estimation errors, artificial noises of different powers are considered, as depicted in Fig. 8. For $\text{SNR} \geq 12$, the distinction between Alice's and Eve's fingerprints is pronounced, enabling accurate transmitter differentiation with all algorithms. At $\text{SNR} = 11$, only the RS algorithm can not accurately identify all fingerprints due to its limited fingerprint selection capability. As $\text{SNR} \leq 10$, decreasing SNR causes Alice's and Eve's fingerprint spaces to increasingly overlap, posing challenges for the PLA model in transmitter identification. Nevertheless, compared to baseline algorithms, the proposed SALU algorithm reduces authentication error rate by 45.45% to 70.00% at $\text{SNR} = 5$. Fig. 8 verifies the robustness of the proposed algorithms against channel estimation errors.

Training complexity. Fig. 9 uses the computational time as a metric to demonstrate the complexity of fingerprint selection algorithms. Due to the need for retraining the GPC-based authentication model for every $(\mathbf{x}_*, \mathbf{y}_*)$, the proposed RO algorithm exhibits the highest complexity. In contrast, leveraging importance sampling in (29) and joint distribution calculation in (30), the proposed (S)ALU algorithms can accelerate the training process. Compared to the ALU algorithm, the SALU algorithm requires additional training time to achieve a lower authentication error rate.

VI. CONCLUSION

To enhance wireless identity security in 6G-enabled IoT, we propose an EGPC-based PLA scheme that innovates over

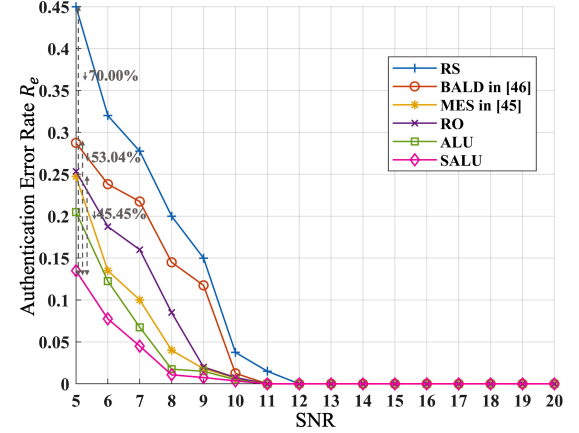


Fig. 8. Error rate difference D_e under the IRS-assisted wireless environment versus different variance of error matrices $\sigma^2 = \sigma_H^2 = \sigma_G^2$.

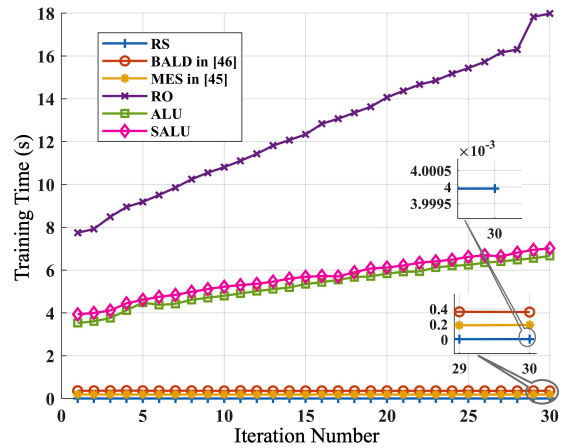


Fig. 9. Training time versus different iteration numbers under the IRS-assisted wireless environment.

state-of-the-art approaches in several key aspects. Firstly, we employ IRSs to enhance fingerprint accuracy in low SNR environments. Secondly, GPs are utilized to model configurable fingerprints, and their posterior distributions are derived for further analysis. Thirdly, we integrate active learning to achieve lightweight cross-layer authentication. We also introduce three fingerprint selection algorithms aimed at improving efficiency. Simulations validate the effectiveness of IRSs and demonstrate the superiority of our proposed algorithms. It is noteworthy that optimizing phase parameters of IRSs remains a topic requiring further exploration, which we intend to investigate using RL methods in future research.

APPENDIX A THE PROOF OF PROPOSITION 1

For the jointly Gaussian random vectors \mathbf{x} and \mathbf{y} , we have

$$\begin{aligned} \begin{bmatrix} \mathbf{x} \\ \mathbf{y} \end{bmatrix} &\sim \mathcal{N} \left(\begin{bmatrix} \boldsymbol{\mu}_x \\ \boldsymbol{\mu}_y \end{bmatrix}, \begin{bmatrix} A & C \\ C^T & B \end{bmatrix} \right) \\ &= \mathcal{N} \left(\begin{bmatrix} \boldsymbol{\mu}_x \\ \boldsymbol{\mu}_y \end{bmatrix}, \begin{bmatrix} \tilde{A} & \tilde{C} \\ \tilde{C}^T & B \end{bmatrix}^{-1} \right). \end{aligned} \quad (38)$$

According to [32], the marginal and conditional distribution of \mathbf{x} are shown as

$$\mathbf{x} \sim \mathcal{N}(\boldsymbol{\mu}_x, A) \quad (39)$$

and

$$\mathbf{x}|\mathbf{y} \sim \mathcal{N}(\boldsymbol{\mu}_x + CB^{-1}(\mathbf{y} - \boldsymbol{\mu}_y), A - CB^{-1}C^T) \quad (40)$$

or

$$\mathbf{x}|\mathbf{y} \sim \mathcal{N}(\boldsymbol{\mu}_x - \tilde{A}^{-1}\tilde{C}(\mathbf{y} - \boldsymbol{\mu}_y), \tilde{A}^{-1}). \quad (41)$$

Thus, **Proposition 1** is proved.

APPENDIX B THE PROOF OF PROPOSITION 2

The product of two Gaussian distributions is represented as

$$\mathcal{N}(\mathbf{x}|\mathbf{a}, A)\mathcal{N}(\mathbf{x}|\mathbf{b}, B) = Z^{-1}\mathcal{N}(\mathbf{x}|\mathbf{c}, C), \quad (42)$$

where

$$\mathbf{c} = C(A^{-1}\mathbf{a} + B^{-1}\mathbf{b}), \quad (43)$$

$$C = (A^{-1} + B^{-1})^{-1}, \quad (44)$$

and

$$Z^{-1} = (2\pi)^{-\frac{D}{2}} |A + B|^{-\frac{1}{2}} \exp\left(-\frac{(\mathbf{a} - \mathbf{b})^T(\mathbf{a} - \mathbf{b})}{2(A + B)}\right). \quad (45)$$

Thus, through multiplying the cavity distribution by t_i from (9), **Proposition 2** is proved.

APPENDIX C THE PROOF OF PROPOSITION 3

Consider

$$Z = \int_{-\infty}^{\infty} \Phi\left(\frac{x - m}{v}\right) \mathcal{N}(x|\mu, \sigma^2) dx, \quad (46)$$

where

$$\Phi(x) = \int_{-\infty}^x \mathcal{N}(y) dy. \quad (47)$$

When $v > 0$, by combining $z = y - x + \mu - m$ and $w = x - \mu$, we can get

$$\begin{aligned} Z_{v>0} &= \frac{\int_{-\infty}^{\infty} \int_{-\infty}^x \exp\left(-\frac{(y-m)^2}{2v^2} - \frac{(x-\mu)^2}{2\sigma^2}\right) dy dx}{2\pi\sigma v} \\ &= \frac{\int_{-\infty}^{\mu-m} \int_{-\infty}^{\infty} \exp\left(-\frac{(z+w)^2}{2v^2} - \frac{w^2}{2\sigma^2}\right) dw dz}{2\pi\sigma v} \end{aligned} \quad (48)$$

and

$Z_{v>0}$

$$\begin{aligned} &= \frac{\int_{-\infty}^{\mu-m} \int_{-\infty}^{\infty} \exp\left(-\frac{1}{2} \begin{bmatrix} w \\ z \end{bmatrix}^T \begin{bmatrix} \frac{1}{v^2} + \frac{1}{\sigma^2} & \frac{1}{v^2} \\ \frac{1}{v^2} & \frac{1}{v^2} \end{bmatrix} \begin{bmatrix} w \\ z \end{bmatrix}\right) 2\pi\sigma v dw dz}{2\pi\sigma v} \\ &= \int_{-\infty}^{\mu-m} \int_{-\infty}^{\infty} \mathcal{N}\left(\begin{bmatrix} w \\ z \end{bmatrix} \mid \mathbf{0}, \begin{bmatrix} \sigma^2 & -\sigma^2 \\ -\sigma^2 & v^2 + \sigma^2 \end{bmatrix}\right) dw dz. \end{aligned} \quad (49)$$

According to (40) and (41), we can get

$$Z_{v>0} = \frac{\int_{-\infty}^{\mu-m} \exp\left(-\frac{z^2}{2(v^2 + \sigma^2)}\right) dz}{\sqrt{2\pi(v^2 + \sigma^2)}} = \Phi\left(\frac{\mu - m}{\sqrt{v^2 + \sigma^2}}\right). \quad (50)$$

When $v < 0$, by combining $\Phi(-z) = 1 - \Phi(z)$ and (46), we can obtain

$$Z_{v<0} = 1 - \Phi\left(\frac{\mu - m}{\sqrt{v^2 + \sigma^2}}\right) = \Phi\left(-\frac{\mu - m}{\sqrt{v^2 + \sigma^2}}\right). \quad (51)$$

By collecting (50) and (51), we can get

$$Z = \int \Phi\left(\frac{x - m}{v}\right) \mathcal{N}(x|\mu, \sigma^2) dx = \Phi(z), \quad (52)$$

where $z = \frac{\mu - m}{v\sqrt{1 + \sigma^2/v^2}} (v \neq 0)$. We aim to get the moments of

$$q(x) = Z^{-1}\Phi\left(\frac{x - m}{v}\right) \mathcal{N}(x|\mu, \sigma^2). \quad (53)$$

By differentiating with respect to μ on (52), we can obtain

$$\begin{aligned} \frac{\partial Z}{\partial \mu} &= \int \frac{x - \mu}{\sigma^2} \Phi\left(\frac{x - m}{v}\right) \mathcal{N}(x|\mu, \sigma^2) dx = \frac{\partial}{\partial \mu} \Phi(z) \\ &\iff \frac{1}{\sigma^2} \int x \Phi\left(\frac{x - m}{v}\right) \mathcal{N}(x|\mu, \sigma^2) dx - \frac{\mu Z}{\sigma^2} \\ &= \frac{\mathcal{N}(z)}{v\sqrt{1 + \sigma^2/v^2}}, \end{aligned} \quad (54)$$

where $\partial\Phi(z)/\partial\mu = \mathcal{N}(z)\partial z/\partial\mu$ is utilized. Multiplying through by σ^2/Z , (55) is obtained.

$$\mathbb{E}_q[x] = \mu + \frac{\sigma^2 \mathcal{N}(z)}{\Phi(z) v \sqrt{1 + \frac{\sigma^2}{v^2}}}. \quad (55)$$

Similarly, we can obtain the second moment as

$$\begin{aligned} \frac{\partial^2 Z}{\partial \mu^2} &= \int \left[\frac{x^2}{\sigma^4} - \frac{2\mu x}{\sigma^4} + \frac{\mu^2}{\sigma^4} - \frac{1}{\sigma^2} \right] \Phi\left(\frac{x - m}{v}\right) \mathcal{N}(x|\mu, \sigma^2) dx \\ &= -\frac{z\mathcal{N}(z)}{v^2 + \sigma^2} \iff \\ \mathbb{E}_q[x^2] &= 2\mu\mathbb{E}_q[x] - \mu^2 + \sigma^2 - \frac{\sigma^4 z \mathcal{N}(z)}{\Phi(z) (v^2 + \sigma^2)}. \end{aligned} \quad (56)$$

By combining (55) and (56), we can get

$$\begin{aligned} \mathbb{E}_q[(x - \mathbb{E}_q[x])^2] &= \mathbb{E}_q[x^2] - \mathbb{E}_q[x]^2 \\ &= \sigma^2 - \frac{\sigma^4 \mathcal{N}(z)}{(v^2 + \sigma^2) \Phi(z)} \left(z + \frac{\mathcal{N}(z)}{\Phi(z)} \right). \end{aligned} \quad (57)$$

Thus, **Proposition 3** is proved.

APPENDIX D THE PROOF OF PROPOSITION 4

We can obtain (19), (20), and (21) according to (43), (44), and (45). Hence, **Proposition 4** is proved.

APPENDIX E THE PROOF OF PROPOSITION 5

The approximated mean for f_* can be denoted as

$$\begin{aligned}\mathbb{E}_q[f_*|X, \mathbf{y}, \mathbf{x}_*] &= \mathbf{k}_*^T K^{-1} \boldsymbol{\mu} \\ &= \mathbf{k}_*^T K^{-1} \left(K^{-1} + \tilde{\Sigma}^{-1} \right)^{-1} \tilde{\Sigma}^{-1} \tilde{\boldsymbol{\mu}} \\ &= \mathbf{k}_*^T \left(K + \tilde{\Sigma} \right)^{-1} \tilde{\boldsymbol{\mu}}.\end{aligned}\quad (58)$$

The variance of $f_*|X, \mathbf{y}$ under the Gaussian approximation can be denoted as

$$\begin{aligned}\mathbb{V}_q[f_*|X, \mathbf{y}, \mathbf{x}_*] &= \mathbb{E}_{p(f_*|X, \mathbf{x}_*, \mathbf{f})} f_* - \mathbb{E}[f_*|X, \mathbf{x}_*, \mathbf{f}]^2 \\ &= k(\mathbf{x}_*, \mathbf{x}_*) - \mathbf{k}_*^T K^{-1} \mathbf{k}_* + \mathbf{k}_*^T K^{-1} \left(K^{-1} + \tilde{\Sigma} \right)^{-1} K^{-1} \mathbf{k}_* \\ &= k(\mathbf{x}_*, \mathbf{x}_*) - \mathbf{k}_*^T \left(K^{-1} + \tilde{\Sigma} \right)^{-1} \mathbf{k}_*.\end{aligned}\quad (59)$$

Then, we can obtain

$$\begin{aligned}q(y_*|X, \mathbf{y}, \mathbf{x}_*) &= \mathbb{E}_q[\pi_*|X, \mathbf{y}, \mathbf{x}_*] \\ &= \int \Phi(f_*) q(f_*|X, \mathbf{y}, \mathbf{x}_*) df_*.\end{aligned}\quad (60)$$

According to (50), we can obtain

$$q(y_*|X, \mathbf{y}, \mathbf{x}_*) = \Phi \left(\frac{\mathbf{k}_*^T \left(K + \tilde{\Sigma} \right)^{-1} \tilde{\boldsymbol{\mu}}}{\sqrt{1 + k(\mathbf{x}_*, \mathbf{x}_*) - \mathbf{k}_*^T \left(K + \tilde{\Sigma} \right)^{-1} \mathbf{k}_*}} \right). \quad (61)$$

By combining (11) and (61), **Proposition 5** is proved.

APPENDIX F THE PROOF OF PROPOSITION 6

Given f_s and f_* , y_s and y_* are conditionally independent. Hence, $p(y_s, y_*|x_s, x_*)$ can be represented as

$$\begin{aligned}p(y_s = 1, y_* = 1|x_s, x_*) &= \iint \Phi(f_s) \Phi(f_*) \phi(f_s, f_*|\mu_{s*}, \Sigma_{s*}) df_s df_* \\ &= \iint \Phi(f_*) \phi(f_*|\tilde{\mu}_*(f_s), \tilde{\sigma}_{**}) df_* \Phi(f_s) \phi(f_s|\mu_s, \sigma_{ss}) df_s \\ &= \int \Phi \left(\frac{\tilde{\mu}_*(f_s)}{\sqrt{\tilde{\sigma}_{**} + 1}} \right) \Phi(f_s) \phi(f_s|\mu_s, \sigma_{ss}) df_s.\end{aligned}\quad (62)$$

Hence, **Proposition 6** is proved.

APPENDIX G THE PROOF OF LEMMA 1

P_{md} and P_{fa} are represented as

$$P_{md} = \frac{FL}{FL + TA} \quad (63)$$

and

$$P_{fa} = \frac{FA}{FA + TA}. \quad (64)$$

R_e is denoted as

$$\begin{aligned}R_e &= \frac{1}{N_a} \sum_{n=1}^{N_a} \mathbb{I}(\mathbf{L}_n \neq \mathbf{Y}_n) \\ &= \frac{FA + FL}{TL + TA + FL + FA} \\ &= \frac{1}{\frac{TL + TA + FL + FA}{FA + FL}} \\ &= \frac{1}{\frac{\frac{TL}{TA} + 1}{\frac{FA}{TA} + \frac{FL}{TA}}} \\ &= \frac{1}{1 + \frac{\frac{TL}{TA}}{\frac{FA}{TA} + \frac{FL}{TA}}}\end{aligned}\quad (65)$$

By combining (63), (64), and (65), **Lemma 1** is proved.

REFERENCES

- [1] J. Wang, M. K. Lim, C. Wang, and M.-L. Tseng, "The evolution of the internet of things (iot) over the past 20 years," *Comput. Ind. Eng.*, vol. 155, p. 107174, 2021.
- [2] Y. Zeng, J. Chen, J. Xu, D. Wu, X. Xu, S. Jin, X. Gao, D. Gesbert, S. Cui, and R. Zhang, "A tutorial on environment-aware communications via channel knowledge map for 6g," *IEEE Commun. Surv. Tutor.*, 2024.
- [3] S. E. Trevlakis, A.-A. A. Boulogiorgos, D. Pliatsios, J. Querol, K. Ntonitin, P. Sarigiannidis, S. Chatzinotas, and M. Di Renzo, "Localization as a key enabler of 6g wireless systems: A comprehensive survey and an outlook," *IEEE Open J. Commun. Soc.*, 2023.
- [4] S. Xia, X. Tao, N. Li, S. Wang, T. Sui, H. Wu, J. Xu, and Z. Han, "Multiple correlated attributes based physical layer authentication in wireless networks," *IEEE Trans. Veh. Technol.*, vol. 70, no. 2, pp. 1673–1687, 2021.
- [5] S. R. Garzon, H. Yildiz, and A. Küpper, "Decentralized identifiers and self-sovereign identity in 6g," *IEEE Netw.*, vol. 36, no. 4, pp. 142–148, 2022.
- [6] 3GPP, "Security architecture and procedures for 5g system, version 17.0.0," 2020.
- [7] N. Xie, J. Zhang, and Q. Zhang, "Security provided by the physical layer in wireless communications," *IEEE Netw.*, 2022.
- [8] I. H. Abdulqader and S. Zhou, "Sliceblock: context-aware authentication handover and secure network slicing using dag-blockchain in edge-assisted sdn/nfv-6g environment," *IEEE Internet Things J.*, vol. 9, no. 18, pp. 18 079–18 097, 2022.
- [9] H. Fang, Z. Xiao, X. Wang, L. Xu, and L. Hanzo, "Collaborative authentication for 6g networks: An edge intelligence based autonomous approach," *IEEE Trans. Inf. Forensic Secur.*, vol. 18, pp. 2091–2103, 2023.
- [10] L. Jin, X. Hu, Y. Lou, Z. Zhong, X. Sun, H. Wang, and J. Wu, "Introduction to wireless endogenous security and safety: Problems, attributes, structures and functions," *China Commun.*, vol. 18, no. 9, pp. 88–99, 2021.
- [11] T. Jing, H. Huang, Q. Gao, Y. Wu, Y. Huo, and Y. Wang, "Multi-user physical layer authentication based on csi using resnet in mobile iiot," *IEEE Trans. Inf. Forensics Secur.*, 2023.
- [12] R. Meng, X. Xu, H. Sun, H. Zhao, B. Wang, S. Han, and P. Zhang, "Multiuser physical-layer authentication based on latent perturbed neural networks for industrial internet of things," *IEEE Internet Things J.*, vol. 10, no. 1, pp. 637–652, 2023.
- [13] R. Meng, X. Xu, H. Zhao, B. Wang, G. Li, B. Xu, and P. Zhang, "Multiobservation-multichannel-attribute-based multiuser authentication for industrial wireless edge networks," *IEEE Trans. Ind. Informat.*, vol. 20, no. 2, pp. 2097–2108, 2024.
- [14] G. Olieri, S. Sciancalepore, S. Raponi, and R. Di Pietro, "Past-ai: Physical-layer authentication of satellite transmitters via deep learning," *IEEE Trans. Inf. Forensics Secur.*, vol. 18, pp. 274–289, 2022.
- [15] N. Xie, Z. Li, and H. Tan, "A survey of physical-layer authentication in wireless communications," *IEEE Commun. Surv. Tutor.*, vol. 23, no. 1, pp. 282–310, 2020.
- [16] V.-L. Nguyen, P.-C. Lin, B.-C. Cheng, R.-H. Hwang, and Y.-D. Lin, "Security and privacy for 6g: A survey on prospective technologies and challenges," *IEEE Commun. Surv. Tutor.*, vol. 23, no. 4, pp. 2384–2428, 2021.

[17] L. Xiao, L. J. Greenstein, N. B. Mandayam, and W. Trappe, "Using the physical layer for wireless authentication in time-variant channels," *IEEE Trans. Commun.*, vol. 7, no. 7, pp. 2571–2579, 2008.

[18] Y. Liu, P. Zhang, Y. Shen, L. Peng, and X. Jiang, "Online machine learning-based physical layer authentication for mmwave mimo systems," *Ad Hoc Networks*, vol. 131, p. 102864, 2022.

[19] A. Chorti, A. N. Barreto, S. Köpsell, M. Zoli, M. Chafii, P. Sehier, G. Fettweis, and H. V. Poor, "Context-aware security for 6g wireless: The role of physical layer security," *IEEE Communications Standards Magazine*, vol. 6, no. 1, pp. 102–108, 2022.

[20] H.-M. Wang and Q.-Y. Fu, "Channel-prediction-based one-class mobile iot device authentication," *IEEE Internet Things J.*, vol. 9, no. 10, pp. 7731–7745, 2022.

[21] F. Xie, Z. Pang, H. Wen, W. Lei, and X. Xu, "Weighted voting in physical layer authentication for industrial wireless edge networks," *IEEE Trans. Ind. Inform.*, vol. 18, no. 4, pp. 2796–2806, 2021.

[22] Y. Chen, P.-H. Ho, H. Wen, S. Y. Chang, and S. Real, "On physical-layer authentication via online transfer learning," *IEEE Internet Things J.*, vol. 9, no. 2, pp. 1374–1385, 2021.

[23] L. Xiao, Y. Li, G. Han, G. Liu, and W. Zhuang, "Phy-layer spoofing detection with reinforcement learning in wireless networks," *IEEE Trans. Veh. Technol.*, vol. 65, no. 12, pp. 10037–10047, 2016.

[24] I. RECOMMENDATION, "Framework and overall objectives of the future development of imt for 2030 and beyond," tech. rep., International Telecommunication Union (ITU) Recommendation (ITU-R), Tech. Rep., 2023.

[25] H. Fang, X. Wang, and L. Hanzo, "Learning-aided physical layer authentication as an intelligent process," *IEEE Trans. Commun.*, vol. 67, no. 3, pp. 2260–2273, 2018.

[26] P. Zhang, Y. Shen, X. Jiang, and B. Wu, "Physical layer authentication jointly utilizing channel and phase noise in mimo systems," *IEEE Trans. Commun.*, vol. 68, no. 4, pp. 2446–2458, 2020.

[27] L. Senigagliesi, M. Baldi, and E. Gambi, "Authentication at the physical layer with cooperative communications and machine learning," in *2022 Joint European Conference on Networks and Communications & 6G Summit (EuCNC/6G Summit)*. IEEE, 2022, pp. 71–76.

[28] L. Xiao, X. Wan, and Z. Han, "Phy-layer authentication with multiple landmarks with reduced overhead," *IEEE Trans. Commun.*, vol. 17, no. 3, pp. 1676–1687, 2017.

[29] R. Meng, X. Xu, B. Wang, H. Sun, S. Xia, S. Han, and P. Zhang, "Physical-layer authentication based on hierarchical variational autoencoder for industrial internet of things," *IEEE Internet Things J.*, vol. 10, no. 3, pp. 2528–2544, 2023.

[30] M. Z. Chen, W. Tang, J. Y. Dai, J. C. Ke, L. Zhang, C. Zhang, J. Yang, L. Li, Q. Cheng, S. Jin *et al.*, "Accurate and broadband manipulations of harmonic amplitudes and phases to reach 256 qam millimeter-wave wireless communications by time-domain digital coding metasurface," *Natl. Sci. Rev.*, vol. 9, no. 1, p. nwab134, 2022.

[31] N. Gao, Y. Han, N. Li, S. Jin, and M. Matthaiou, "When physical layer key generation meets ris: Opportunities, challenges, and road ahead," *IEEE Wirel. Commun.*, 2024.

[32] C. K. Williams and C. E. Rasmussen, *Gaussian processes for machine learning*. MIT press Cambridge, MA, 2006, vol. 2, no. 3.

[33] Y. Zhu, B. Mao, and N. Kato, "Intelligent reflecting surface in 6g vehicular communications: A survey," *IEEE Open J. Veh. Technol.*, vol. 3, pp. 266–277, 2022.

[34] B. Settles, *Active learning literature survey*. University of Wisconsin-Madison Department of Computer Sciences, 2009.

[35] S. Tomasin, H. Zhang, A. Chorti, and H. V. Poor, "Challenge-response physical layer authentication over partially controllable channels," *IEEE Commun. Mag.*, vol. 60, no. 12, pp. 138–144, 2022.

[36] Y. Wang, H. Lu, D. Zhao, Y. Deng, and A. Nallanathan, "Wireless communication in the presence of illegal reconfigurable intelligent surface: Signal leakage and interference attack," *IEEE Wirel. Commun.*, vol. 29, no. 3, pp. 131–138, 2022.

[37] B. Zheng, C. You, W. Mei, and R. Zhang, "A survey on channel estimation and practical passive beamforming design for intelligent reflecting surface aided wireless communications," *IEEE Commun. Surv. Tutor.*, vol. 24, no. 2, pp. 1035–1071, 2022.

[38] L. A. Dalton and E. R. Dougherty, "Optimal classifiers with minimum expected error within a bayesian framework—part i: Discrete and gaussian models," *Pattern Recognit.*, vol. 46, no. 5, pp. 1301–1314, 2013.

[39] B.-J. Yoon, X. Qian, and E. R. Dougherty, "Quantifying the objective cost of uncertainty in complex dynamical systems," *IEEE Trans. Signal Process.*, vol. 61, no. 9, pp. 2256–2266, 2013.

[40] G. Zhao, E. Dougherty, B.-J. Yoon, F. Alexander, and X. Qian, "Efficient active learning for gaussian process classification by error reduction," *Advances in Neural Information Processing Systems*, vol. 34, pp. 9734–9746, 2021.

[41] N. Roy and A. McCallum, "Toward optimal active learning through monte carlo estimation of error reduction," *ICML, Williamstown*, vol. 2, pp. 441–448, 2001.

[42] G. Zhao, E. Dougherty, B.-J. Yoon, F. J. Alexander, and X. Qian, "Bayesian active learning by soft mean objective cost of uncertainty," in *International Conference on Artificial Intelligence and Statistics*. PMLR, 2021, pp. 3970–3978.

[43] 3GPP, "Study on channel model for frequencies from 0.5 to 100 ghz, version 17.0.0," 2022.

[44] X. Hu, C. Masouros, and K.-K. Wong, "Reconfigurable intelligent surface aided mobile edge computing: From optimization-based to location-only learning-based solutions," *IEEE Trans. Commun.*, vol. 69, no. 6, pp. 3709–3725, 2021.

[45] P. Sebastiani and H. P. Wynn, "Maximum entropy sampling and optimal bayesian experimental design," *Journal of the Royal Statistical Society: Series B (Statistical Methodology)*, vol. 62, no. 1, pp. 145–157, 2000.

[46] N. Housby, F. Huszár, Z. Ghahramani, and M. Lengyel, "Bayesian active learning for classification and preference learning," *arXiv preprint arXiv:1112.5745*, 2011.